Support of this work by the National Science Foundation (CHE8711736) and the Petroleum Research Fund administered by the American Chemical Society (PRF15461-A66-C) is gratefully acknowledged.

References

GAO, Y., GAJHEDE, M., MALLINSON, P., PETŘÍČEK, V. & COPPENS, P. (1988). *Phys. Rev. B*, **37**, 1825-1831.

International Tables for Crystallography. (1983). Vol. A. Dordrecht: Reidel. (Present distributor Kluwer Academic Publishers, Dordrecht.)

KUCHARCZYK, D., PACIOREK, W. A. & USZYNSKI, I. (1986). Abstr. Proc. Int. Conf. on Polytypes and Modulated Structures, Wrocław, Poland, p. 79.

PETŘÍČEK, V. (1986). Abstr. Proc. Int. Conf. on Polytypes and Modulated Structures, Wrocław, Poland, pp. 46-47.

PETŘÍČEK, V., COPPENS, P. & BECKER, P. J. (1985). *Acta Cryst.* A**41**, 478-483.

WOLFF, P. M. DE (1974). *Acta Cryst.* A**30**, 777-785.

WOLFF, P. M. DE, JANSSEN, T. & JANNER, A. (1981). *Acta Cryst.* A**37**, 625-636.

YAMAMOTO, A. (1980). *Phys. Rev. B*, **22**, 373-379.

YAMAMOTO, A. (1983). *Phys. Rev. B*, **27**, 7823-7825.

Acta Cryst. (1988). A**44**, 1055-1059

Plane-Wave Theory of Three-Crystal Laue Interferometer

BY R. COLELLA

Department of Physics, Purdue University, West Lafayette, IN 47907, *USA*

(*Received* 5 *April* 1988; *accepted* 22 *June* 1988)

Dedicated to Professor U. Bonse on the occasion of his 60th birthday

Abstract

The plane-wave theory of a three-crystal Laue interferometer is presented in terms of the amplitudes diffracted by a single slab in the Laue case, using Zachariasen's formalism. Successive applications of the single-slab expressions for the amplitudes lead to the final intensities of the interfering beams present on the back side of the third crystal slab. Numerical examples for X-ray and neutron diffraction show clearly the different contrast relationships in the two cases.

1. Introduction

The theory of a three-crystal symmetric Laue interferometer for spherical waves, in the case of zero absorption (neutrons or X-rays), has been developed by Bauspiess, Bonse & Graeff (1976). Such a theory contains the plane-wave situation as a particular case. An equivalent treatment, with full consideration of absorption, has also been presented by Petrascheck (1979).

Other treatments have appeared in the literature for the plane-wave situation (Bonse & Hart, 1965; Bonse & te Kaat, 1971) and zero or small absorption, for applications to neutron diffraction (Rauch & Suda, 1974; Staudenmann, Werner, Colella & Overhauser, 1980).

The spherical-wave treatment enables one to evaluate the intensity distribution as a function of position on the back of the third crystal slab of the interferometer. While such information is valuable in evaluating the overall performance of an interferometer in terms of the residual strain resulting from crystal defects and fastening techniques, quite often in designing an interferometer the attention is concentrated on the overall counting rate, namely on the integrated intensity emerging from the third slab, for which a plane-wave theory is adequate. Parseval's theorem, in fact, assures us that the integrated intensities are the same whether a plane- or a spherical-wave treatment is employed (Kato, 1968).

In this paper we present a very simple and straightforward derivation for the integrated intensities of some of the beams present behind the third slab of an interferometer made up with three slabs set for Laue diffraction (asymmetric), with full consideration of absorption, so that the formalism can be used in the X-ray case when absorption is important.

We will treat the case of a single slab first, and derive expressions that will then be combined in such a way as to obtain in a straightforward fashion the amplitudes of the waves multiply diffracted by a stack of crystal slabs, as a function of a global phase shift β, introduced along one of the interfering beams. The only critical assumption here is that all the various slabs are exactly coherent in space, which is true when monolithic interferometers are used.

Use will be made throughout this paper of the dynamical theory formalism developed by

0108-7673/88/061055-05$03.00

Zachariasen (1945), for the basic expressions of the amplitudes diffracted and transmitted by a crystal slab in the Laue case.

2. Diffraction through one slab only

We will consider in this section the situation depicted in Fig. 1. O_i and H_i are amplitudes of vacuum plane waves *incident* on the crystal. O_f and H_f are amplitudes of vacuum plane waves *leaving* the crystal. The vacuum wave vector $\mathbf{K}_0$ associated with O_i is chosen in such a way as to excite a strong Bragg reflection $\mathbf{B}_H$ inside the crystal. The wave vector $\mathbf{K}_H$ associated with H_i is defined by

$$\begin{aligned} \mathbf{K}_H^t &= \mathbf{K}_0^t + \mathbf{B}_H^t \\ K_H &= K_0 = 1/\lambda \end{aligned} \tag{1}$$

where the superscript t indicates the tangential component on the crystal surface. The vacuum wave vectors associated with the O_f and H_f beams are identical to $\mathbf{K}_0$ and $\mathbf{K}_H$, respectively.

Note that in Fig. 1 only one wave field is depicted, propagating normal to the slab. In reality there are in general two wave fields, with directions of propagations within $\mathbf{K}_0$ and $\mathbf{K}_H$ (approximately) for each direction of incidence, corresponding to the two normals to the dispersion surface at the two tie-points (Batterman & Cole, 1964). For the sake of simplicity in drawing Fig. 1 and for the purpose of this discussion we can consider only one wave field without loss of generality. The formulae derived later will of course include both wave fields.

2.1. *First case*; O_i *only is present*

We first consider the case in which only one beam is incident on the entrance surface, with wave vector $\mathbf{K}_0$. Following the customary procedure of neglecting refraction effects at the surface, the boundary conditions require the vacuum electric field and the crystal displacement field to be equal, and can be written

$$\begin{aligned} O_i &= D_{01} + D_{02} \\ 0 &= x_1 D_{01} + x_2 D_{02} \end{aligned} \tag{2}$$

where D_{01} and D_{02} are the two amplitudes of the electric displacement inside the crystal, and x_1, x_2 are the ratios D_{H1}/D_{01}, D_{H2}/D_{02} defined in Zachariasen's (1945) book (equations 3·121-3·126). Solving the system of equations (2) we obtain

$$\begin{aligned} D_{01} &= O_i x_2/(x_2 - x_1); \\ D_{02} &= -O_i x_1/(x_2 - x_1). \end{aligned} \tag{3}$$

The boundary conditions at the exit surface are

$$O_f = O_i \exp(-2\pi i K_{0n} b) \frac{x_2 c_1 - x_1 c_2}{x_2 - x_1} \tag{4a}$$

$$H_f = O_i \exp[-2\pi i (K_{0n} + B_{Hn}) b] \frac{x_2 x_1 (c_1 - c_2)}{x_2 - x_1}, \tag{4b}$$

where K_{0n} and B_{Hn} are given by $\mathbf{K}_0 \cdot \mathbf{n}$ and $\mathbf{B}_H \cdot \boldsymbol{n}$, respectively, $\mathbf{n}$ is a unit vector normal to the crystal slab, pointing inside the entrance surface, b is the thickness, and c_1, c_2 are the exponential factors defined by Zachariasen (equations 3·121-3·126):

$$c_i = \exp(-2\pi i \delta_0^i K_0^2 b / K_{0n}),$$

where δ_0^i are the eigenvalues associated with the crystal wave vector β_0 when a Bragg reflection is excited.

2.2. *Second case*; H_i *only is present*

We now consider the case in which the only incident wave is along the direction of the diffracted beam, with wave vector $\mathbf{K}_H$. The boundary conditions on the entrance surface now give

$$\begin{aligned} 0 &= D_{01} + D_{02} \\ H_i &= x_1 D_{01} + x_2 D_{02} \end{aligned} \tag{5}$$

$$\begin{aligned} D_{01} &= -H_i (x_2 - x_1)^{-1}; \\ D_{02} &= H_i (x_2 - x_1)^{-1}. \end{aligned} \tag{6}$$

At the exit surface,

$$O_f = H_i \exp(-2\pi i K_{0n} b) \frac{c_2 - c_1}{x_2 - x_1} \tag{7a}$$

$$H_f = H_i \exp[-2\pi i (K_{0n} + B_{Hn}) b] \frac{x_2 c_2 - x_1 c_1}{x_2 - x_1}. \tag{7b}$$

2.3. *Third case*; O_i *and* H_i *are present*

The boundary conditions at the entrance surface give

$$\begin{aligned} O_i &= D_{01} + D_{02} \\ H_i &= x_1 D_{01} + x_2 D_{02} \end{aligned} \tag{8}$$

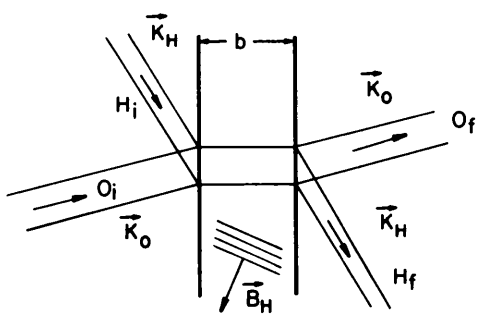

Fig. 1. Laue diffraction through a single slab. The vacuum wave vectors for the O and H beams are identical on both sides. For the sake of clarity, only one wave field inside the crystal is shown, propagating perpendicular to the slab.

from which we get

$$D_{01} = (O_i x_2 - H_i)/(x_2 - x_1)$$
$$D_{02} = (H_i - O_i x_1)/(x_2 - x_1). \tag{9}$$

At the exit surface we get

$$O_f = \exp(-2\pi i K_{0n} b) \times (O_i x_2 c_1 - H_i c_1 + H_i c_2 - O_i x_1 c_2)/(x_2 - x_1) \tag{10a}$$

$$H_f = \exp[-2\pi i(K_{0n} + B_{Hn})b] \times (O_i x_1 x_2 c_1 - H_i x_1 c_1 + H_i x_2 c_2 - O_i x_1 x_2 c_2) \times (x_2 - x_1)^{-1}. \tag{10b}$$

We notice that both O_f and H_f consist basically of two terms, one due to O_i only, and another one due to H_i only.

3. Diffraction through three parallel equidistant slabs

We will now consider the situation depicted in Fig. 2, corresponding to a standard LLL interferometer. The nomenclature of the various beams is transparent from the figure. Again, we only show one particular wave field, propagating normal to the slabs. Since we are considering a monolithic interferometer, the resonance error (James, 1962) is the same in all crystals, so the direction of propagation of the wave field shown in the figures is the same in all three slabs.

It is important to note at this point that the amplitudes O_1, H_1, H_{11}^U, O_{11}^L, H_{11}^L, O_f, H_f of the beams shown in Fig. 2 are all defined *at the exit surfaces* of the three slabs, and are all related to *vacuum waves.* The unlabeled beams are not considered in the foregoing treatment.

From (4)

$$H_{11}^U = \frac{x_1 x_2 (x_2 c_1 - x_1 c_2)}{(x_2 - x_1)^2}(c_1 - c_2) \times \exp[-2\pi i K_{0n}(a + 2b)] \exp(-2\pi i B_{Hn} b) \tag{11}$$

where a is the distance between the slabs.

From (4b) and (7a),

$$O_{11}^L = \frac{-x_1 x_2 (c_2 - c_1)^2}{(x_2 - x_1)^2} \times \exp[-2\pi i(2K_{0n} + B_{Hn})b] \exp(-2\pi i K_{hn} a) \tag{12}$$

where

$$K_{hn} = \mathbf{K}_h \cdot \mathbf{n} = [1/\lambda^2 - (K_H^t)^2]^{1/2}$$

and K_H^t is given by (1).

Let O_{fO} be the contribution to O_f due to O_{11}^L, and O_{fH} the same contribution due to H_{11}^U.

From (4a) and (12),

$$O_{fO} = \frac{-x_1 x_2 (c_2 - c_1)^2 (x_2 c_1 - x_1 c_2)}{(x_2 - x_1)^3} \times \exp[-2\pi i(3K_{0n} + B_{Hn})b] \times \exp[-2\pi i(K_{0n} + K_{Hn})a]. \tag{13}$$

From (7a) and (11),

$$O_{fH} = \frac{-x_1 x_2 (c_2 - c_1)^2 (x_2 c_1 - x_1 c_2)}{(x_2 - x_1)^3} \times \exp[-2\pi i(3K_{0n} + B_{Hn})b] \times \exp[-2\pi i(K_{0n} + K_{Hn})a]. \tag{14}$$

It is therefore shown (important result) that O_{fO} and O_{fH} *are identical.* This result could be anticipated by noting that each photon in O_i takes the same 'bounces' before going into O_f. If a phase shift, say β, is introduced along one of the two interfering beams (H_{11}^U or O_{11}^L), the intensity of O_f will be

$$|O_f|^2 = |O_{fO}(1 + e^{i\beta})|^2 = 2|O_{fO}|^2(1 + \cos\beta), \tag{15}$$

which shows that, in an ideal interferometer, the intensity of the O_f beam varies between a maximum value and zero.

We now proceed to evaluate H_f. Again we consider the two separate contributions, H_{fO} (due to O_{11}^L) and H_{fH} (due to H_{11}^U).

From (4b) and (12),

$$H_{fO} = \frac{(x_1 x_2)^2 (c_2 - c_1)^3}{(x_2 - x_1)^3} \times \exp[-2\pi i(3K_{0n} + B_{Hn})b] \times \exp[-2\pi i(K_{0n} + K_{Hn})a]. \tag{16}$$

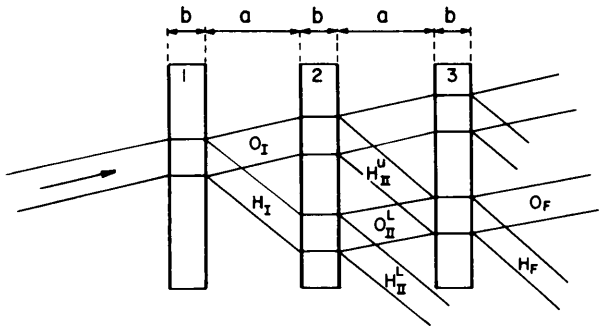

Fig. 2. Laue-case diffraction through three crystal slabs. The interfering beams are labeled O_f and H_f. The unlabeled beams on the right side of the third slab are not considered in the analysis given in this paper.

From (7*b*) and (11),

$$H_{fH} = \frac{x_1x_2(x_2c_1 - x_1c_2)(c_1 - c_2)(x_2c_2 - x_1c_1)}{(x_2 - x_1)^3} \times \exp[-2\pi i(3K_{0n} + 2B_{Hn})b] \times \exp[-2\pi i(K_{0n} + K_{Hn})a] \quad (17)$$

$$|H_f|^2 = |H_{fO} + e^{i\beta}H_{fH}|^2. \quad (18)$$

We see now that H_{fO} and H_{fH} are no longer identical. Therefore, even when $\beta = \pi$, H_f is not zero, which means that the intensity of H_f varies between two finite values.

The fringe contrast is always greater for the O_f beam, which is in general the most interesting beam in almost all experimental situations involving interferometers.

Let

$$H^*_{fO}H_{fH} = \rho\, e^{i\delta}.$$

Then

$$|H_f|^2 = |H_{fO}|^2 + |H_{fH}|^2 + 2\rho\cos\delta\cos\beta - 2\rho\sin\delta\sin\beta. \quad (19)$$

Another interesting quantity to evaluate is the intensity of the beam called H^L_{II} in Fig. 2. This beam escapes the interferometer if the third slab is not too big, it does not exhibit interferential effects, and is sometimes used to adjust the interferometer at the correct Bragg angle.

From (4*b*) and (7*b*),

$$H^L_{II} = \frac{(c_1 - c_2)(x_2c_2 - x_1c_1)x_2x_1}{(x_2 - x_1)^2} \times \exp[-2\pi i(2K_{0n} + 2B_{Hn})b] \times \exp(-2\pi iK_{Hn}a). \quad (20)$$

It is convenient at this point to integrate with respect to θ, the angle of incidence, since we are interested in integrated intensities.

Let

$$R_{Of} = \int_{-\infty}^{+\infty} |O_f|^2\,d\theta, \quad R_{Hf} = \int_{-\infty}^{+\infty} |H_f|^2\,d\theta,$$

$$R^L_{H\,II} = \int_{-\infty}^{+\infty} |H^L_{II}|^2\,d\theta,$$

$$A = \int_{-\infty}^{+\infty} |O_{fO}|^2\,d\theta, \quad B = \int_{-\infty}^{+\infty} (|H_{fO}|^2 + |H_{fH}|^2)\,d\theta,$$

$$C = \int_{-\infty}^{+\infty} (\rho\cos\delta)\,d\theta, \quad D = \int_{-\infty}^{+\infty} (\rho\sin\delta)\,d\theta.$$

We finally obtain

$$R_{Of} = 2A(1 + \cos\beta)$$

$$R_{Hf} = B + 2C\cos\beta - 2D\sin\beta.$$

4. Numerical examples*

Let us consider a neutron interferometer, with $\lambda = 1{\cdot}42$ Å; slab thickness $t = 2$ mm; $hkl = 220$.

$$R_{Of} = 8{\cdot}31\times10^{-7}(1 + \cos\beta)$$

$$R_{Hf} = 2{\cdot}12\times10^{-6} - 8{\cdot}31\times10^{-7}\cos\beta - 8{\cdot}03\times10^{-12}\sin\beta$$

$$R^L_{H\,II} = 1{\cdot}85\times10^{-6}.$$

Note that the last term of R_{Hf} is negligible, and that the fringe contrast in R_{Hf} is reversed with respect to R_{Of}, in other words, when $\cos\beta = -1$, $R_{Of} = 0$ and R_{Hf} = maximum. This result was expected, because thermal neutrons suffer negligible absorption in silicon, and the reversal in contrast is a consequence of conservation of neutrons. The contrast reversal can be seen, for example, in the first neutron fringe pattern observed by Rauch, Treimer & Bonse (1974), Fig. 2. On the contrary, if we consider the same interferometer with Mo $K\alpha$ X-rays, $\lambda = 0{\cdot}711$ Å, $hkl = 220$,

$$R_{Of} = 8{\cdot}58\times10^{-8}(1 + \cos\beta)$$

$$R_{Hf} = 7{\cdot}40\times10^{-8} + 6{\cdot}76\times10^{-8}\cos\beta - 1{\cdot}81\times10^{-11}\sin\beta$$

$$R^L_{H\,II} = 6{\cdot}96\times10^{-7}.$$

We now see that, again, the third term in R_{Hf} is negligible, and that the $\cos\beta$ term now appears with a plus sign. The fringe pattern of R_{Hf} is now *in phase* with that of R_{Of}. Since absorption is important with X-rays, conservation of photons does not hold any more. It is also apparent from the last numerical example that the fringe contrast and the intensity of R_{Hf} are not too different from those of R_{Of}, all of which has been observed experimentally in many laboratories, including our own.

The last example is similar to the previous case, except that the 440 reflection is now considered.

* The integrands involved in evaluating, by numerical integration, R_{Of}, R_{Hf}, $R^L_{H\,II}$, A, B, C and D exhibit a rapidly oscillating behavior on the sides of the central peak, when absorption is close to zero. This may cause some problems in evaluating those integrals by computer. The same problem arises in standard two-beam dynamical theory, in which the fast oscillating terms are averaged out (Zachariasen, 1945, equations 3·150, 3·155). When dealing with an interferometer a similar procedure could be adopted, but it does not seem the right thing to do. Averaging out the oscillating terms is equivalent to assuming a thickness roughness Δt of the order of the *Pendellösung* length. In effect, in order for an interferometer to work, the crystals slabs must be polished to a small fraction of a *Pendellösung* length. A correct approach would be to apply the averaging procedure only to the sides of the central peak. An easy way out is to use the integrand expressions as they are, and to repeat the numerical computations several times by randomly shifting (using random-number generators) the integration mesh with respect to the θ axis, and then taking average values.

The values are

$$R_{Of} = 9{\cdot}14 \times 10^{-9}(1 + \cos\beta)$$
$$R_{Hf} = 7{\cdot}96 \times 10^{-9} + 6{\cdot}99 \times 10^{-9}\cos\beta - 3{\cdot}89 \times 10^{-12}\sin\beta$$
$$R^{L}_{H\,II} = 1{\cdot}52 \times 10^{-7}.$$

The fringe pattern is essentially the same as for the 220 reflection, except that the intensities are much weaker.

In conclusion, we have shown how the fringe pattern and all relevant intensities for a LLL interferometer can be obtained by repeated applications of the expressions for the amplitudes obtained for diffraction through a single slab. The neutron and the X-ray cases can both be treated with the same formalism, provided the appropriate parameters are introduced. The treatment is given in terms of plane waves, which is appropriate if global integrated intensities (*i.e.* counting rates) are of interest, rather than spatial intensity distributions across the beams emerging from the last crystal of the interferometer.

This work was supported by the National Science Foundation, Grant DMR-8715503.

References

BATTERMAN, B. W. & COLE, H. (1964). *Rev. Mod. Phys.* **36**, 681-717.
BAUSPIESS, W., BONSE, U. & GRAEFF, W. (1976). *J. Appl. Cryst.* **9**, 68-80.
BONSE, U. & HART, M. (1965). *Z. Phys.* **188**, 154-164.
BONSE, U. & TE KAAT, E. (1971). *Z. Phys.* **243**, 14-45.
KATO, N. (1968). *J. Appl. Phys.* **39**, 2231-2237.
JAMES, R. W. (1962). *The Optical Principles of the Diffraction of X-rays*, p. 70. Ithaca: Cornell Univ. Press.
PETRASCHECK, D. (1979). *Neutron Interferometry*. Proceedings of an International Workshop held 5-7 June 1978 at the Institut Max von Laue-Paul Langevin, Grenoble, edited by U. BONSE & H. RAUCH, pp. 108-134. Oxford: Clarendon Press.
RAUCH, H. & SUDA, M. (1974). *Phys. Status Solidi A*, **25**, 495-505.
RAUCH, H., TREIMER, W. & BONSE, U. (1974). *Phys. Lett. A*, **47**, 369-371.
STAUDENMANN, J. L., WERNER, S. A., COLELLA, R. & OVERHAUSER, A. W. (1980). *Phys. Rev.* **21**, 1419-1438.
ZACHARIASEN, W. H. (1945). *Theory of X-ray Diffraction in Crystals*, inc. Sect. III. New York: John Wiley.

Acta Cryst. (1988). A**44**, 1059-1065

X-ray Powder Diffraction of Anthracene at Hydrostatic Pressures up to 0·9 GPa

BY R. PUFALL AND J. KALUS

Experimentalphysik I der Universität Bayreuth, Postfach 101252, *D*-8580 *Bayreuth, Federal Republic of Germany*

(*Received* 3 *February* 1988; *accepted* 22 *June* 1988)

Abstract

An X-ray powder diffraction cell for pressures up to 0·9 GPa was constructed. The pressure dependence of the unit-cell parameters and pressure-induced changes of the orientation of anthracene molecules were determined at ambient temperature. The diffraction patterns were analysed with a modified Rietveld program. The comparison with calculations based on atom-atom potentials (6-exp-type) between rigid molecules using Williams's [*J. Chem. Phys.* (1967). **47**, 4680-4684] and Kitaigorodski's [*J. Chim. Phys. Phys. Chim. Biol.* (1966). **63**, 9-16] parameters shows that satisfactory agreement can be obtained with the predictions.

I. Introduction

Anthracene crystallizes in space group $P2_1/a$ (C^5_{2h}) with two molecules in the unit cell. There is no phase change at room temperature at the pressures used in our experiment.

The crystalline structure of anthracene is mainly determined by weak van der Waals-like forces, whereas the binding within the molecule is provided by strong covalent bonds. For this reason the planar shape of the molecule remains essentially unchanged when it is incorporated into a crystal lattice. The distances between the molecules are changed under pressure. Therefore it is possible to probe the shape of intermolecular forces or potentials. It turns out that, apart from distances, the orientations of molecules are altered too. Both effects can be seen in elastic scattering *via* accurate determination of Bragg intensities as a function of pressure. This method is in a way complementary to inelastic neutron scattering where information about the intermolecular forces can be deduced from measured phonon dispersion curves. The advantage of inelastic neutron scattering experiments stems from the fact that more experimental data are available to fit a model.

In the next sections we report the experimental details, the results of the powder diffraction

0108-7673/88/061059-07$03.00